Single quark polarization in quantum chromodynamics subprocesses

W. G. D. Dharmaratna
Department of Physics, University of Ruhuna, Matara, Sri Lanka

Gary R. Goldstein
Department of Physics, Tufts University, Medford, Massachusetts 02155
(Received 29 August 1995)

It is well known that the single-polarization asymmetries vanish in QCD with massless quarks. But, heavy quarks with a nonzero mass should be transversely polarized due to the breakdown of the helicity conservation. In this paper we give the exact fourth-order perturbative QCD predictions for the transverse polarization from all QCD subprocesses, $q+q' \to q+q'$, $q+g \to q+g$, $g+g \to q+\bar{q}$, and $q+\bar{q} \to q'+\bar{q}'$, which are significant for heavy quark production, with a description of the method of calculation. The kinematical dependence of the polarization is discussed. Top quark polarization from gluon fusion and quark annihilation processes, which are the important subprocesses at high energies, is estimated and its significance is discussed.

PACS number(s): 12.38.Bx, 13.88.+e

It is well known that in QCD with massless quarks (and gluons) the quark helicity is conserved at each vertex, and so there can be no single-quark polarization in any perturbatively calculated scattering process. This is a phenomenologically significant statement for any hadronic process in which the relevant energies and transverse momenta are large compared to quark "mass" scales. What sets such mass scales is a long-standing question in QCD applications. It is foreshadowed by the distinctions made between current and constituent quark masses in pre-QCD quark and parton models. Whatever the appropriate definition of the quark mass, whether current, constituent, effective, or running mass, once this parameter is nonzero the strict helicity conservation breaks down. And with the possibility of helicity flip vertices, single-quark polarization can occur in scattering processes.

The observation of single-quark polarization, if it were possible in spite of confinement, would signal the importance of quark masses as well as higher-order QCD corrections. The latter is necessitated by the dependence of single-quark polarization on an interference between opposite helicities, which requires, in turn, imaginary parts of bilinear products of amplitudes. Imaginary or complex amplitudes arise from loop diagrams, i.e., beyond the tree level. While it is clear that direct observation of quark polarization is not possible, there are many indirect measures of the putative quantity, such as the polarization or density matrix elements of leading hadrons [1] or the distribution of hadrons in jet fragmentation [2].

Given the fundamental nature of QCD and quark spin, we have been collecting together QCD perturbation theory predictions for single massive quark polarization in some two-body processes. Below we present the results for various flavor combinations in quark-quark scattering, quark-gluon scattering, quark-antiquark annihilation and gluon fusion. The technique for obtaining these results is straightforward. We first calculate the lowest-order Feynman diagrams for the particular process and project out the helicity amplitudes. Then we calculate all the diagrams that contribute an imaginary part in second order in α_s, the strong fine-structure constant. Those imaginary parts all involve similar integrations using the Cutkosky rules. The imaginary contributions to the helicity amplitudes are then projected out and inserted into the relevant expression for the polarization. The one-loop calculations are lengthy and are facilitated by symbolic manipulation software, but are quite well defined.

To make the procedure more concrete we will sketch the calculation of the QCD analogue of electron-muon scattering, $q+q' \to q+q'$. The lowest-order diagram is just one-gluon exchange as shown in Fig. 1(a). The $\mathcal{M}$ matrix for that diagram can be written as

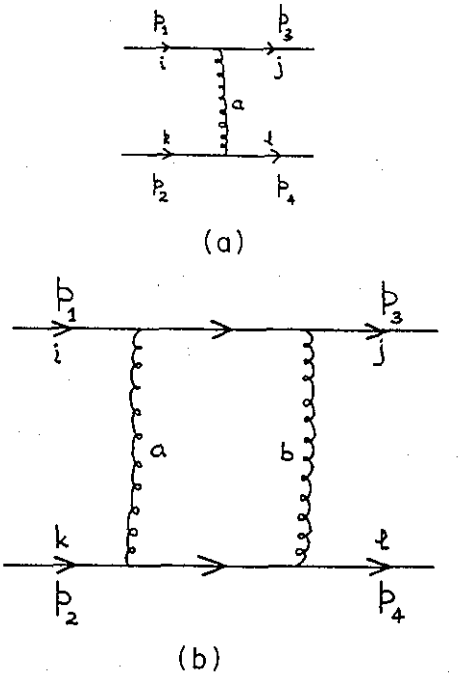

FIG. 1. Lowest-order (a) and fourth-order (b) Feynman diagrams for the $q+q' \to q+q'$ scattering process. In the fourth order only the diagrams which contribute to the polarization are shown.

$$\mathcal{M} = \frac{g^2 \lambda^a_{ij} \lambda^a_{kl}}{q^2} [\bar{u}(p_3)\gamma^\mu u(p_1)][\bar{u}(p_4)\gamma_\mu u(p_2)] \ , \tag{1}$$

where the indices and momenta are indicated in Fig. 1(a) and $q^2 = (p_1 - p_3)^2$. The resultant six independent helicity flip amplitudes,

$$\Phi_1(++ \to ++) \ ,$$

$$\Phi_2(++ \to --) \ ,$$

$$\Phi_3(+- \to +-) \ ,$$

$$\Phi_4(+- \to -+) \ ,$$

$$\Phi_5(++ \to -+) \ ,$$

$$\Phi_6(+- \to ++) \ ,$$

can be expressed in the form

$$\phi_\alpha = \frac{g^2 \lambda^a_{ij} \lambda^a_{kl}}{q^2} f_\alpha \ . \tag{2}$$

The f_α's are given by

$$f_1 = 8p^2 - 4(p^2 - E_1E_2)\cos^2\frac{\theta}{2}, \quad f_4 = 4m_1m_2\sin^2\frac{\theta}{2} \ ,$$

$$f_2 = -4m_1m_2\sin^2\frac{\theta}{2}, \quad f_5 = -4m_1E_2\cos\frac{\theta}{2}\sin\frac{\theta}{2} \ ,$$

$$f_3 = 4(p^2 + E_1E_2)\cos^2\frac{\theta}{2}, \quad f_6 = -4m_2E_1\cos\frac{\theta}{2}\sin\frac{\theta}{2} \ ,$$

where the symbols E_1, E_2, p, and θ defined in the center-of-mass frame are the energy of q, the energy of q', the momentum and the scattering angle, respectively. The next order imaginary contribution is shown in Fig. 1(b). There is only one Feynman diagram that contributes to the imaginary part in the s-channel physical region, the box diagram. The $\mathcal{M}$ matrix for that diagram is

$$\mathcal{M} = -ig^4(\lambda^a\lambda^b)_{ij}(\lambda^a\lambda^b)_{kl}\int \frac{d^4k}{(2\pi)^4}\left(\bar{u}(p_3)\gamma^\nu \frac{\not{p}_1 - \not{k} + m_1}{(p_1-k)^2 - m_1^2}\gamma^\mu u(p_1)\right)$$
$$\times \frac{1}{(k^2 - \delta_m^2)[(k-q)^2 - \delta_m^2]}\left(\bar{u}(p_4)\gamma_\nu \frac{\not{p}_2 + \not{k} + m_2}{(p_2+k)^2 - m_2^2}\gamma_\mu u(p_2)\right) \ , \tag{3}$$

which contains the integration over the internal four-momentum k of the loop, and with δ_m, a gluon mass cutoff that protects against infrared divergences, which will be taken to zero (since such divergences cancel out of the final physical result). First, the k-dependent terms can be separated as

$$\mathcal{M} = \frac{-g^4}{(2\pi)^4}(\lambda^a\lambda^b)_{ij}(\lambda^a\lambda^b)_{kl}\{4p_1\cdot p_2(\gamma^\nu \otimes \gamma_\nu)b - 2[(\gamma^\nu\gamma^\kappa \not{p}_2 \otimes \gamma_\nu) - (\gamma^\nu \otimes \gamma_\nu\gamma^\kappa \not{p}_1)]b_\kappa - (\gamma^\nu\gamma^\kappa\gamma^\mu \otimes \gamma_\nu\gamma^\rho\gamma_\mu)b_{\kappa\rho}\} \ , \tag{4}$$

where the notation $(A \otimes B) = [\bar{u}(p_3)A(p_1)][\bar{u}(p_4)Bu(p)2)]$ is used and

$$(b; b_\kappa; b_{\kappa\rho}) = i\int \frac{d^4k(1; k_\kappa; k_\kappa k_\rho)}{(k^2 - \delta_m^2)((k-q)^2 - \delta_m^2)((p_1-k)^2 - m_1^2)((p_2+k)^2 - m_2^2)} \ . \tag{5}$$

The imaginary part (or the discontinuity across the unitarity cut in the physical s channel) is obtained from the Cutkosky rules by replacing the two direct channel propagators with on-shell δ functions:

$$\frac{1}{(p_1-k)^2 - m_1^2} \Longrightarrow 2\pi i\delta((p_1-k)^2 - m_1^2)\theta((p_1-k)^0) \ ,$$
$$\frac{1}{(p_2+k)^2 - m_2^2} \Longrightarrow 2\pi i\delta((p_2+k)^2 - m_2^2)\theta((p_2-k)^0) \ ,$$

where the θ functions take the positive-energy parts. This replacement puts the particles corresponding to the intermediate states on their positive-energy mass shell. Equation (5) becomes

$$(b; b_\kappa; b_{\kappa\rho})_{\text{cut}} = i(2\pi i)^2\int \frac{d^4k(1; k_\kappa; k_{\kappa\rho})\delta((p_1-k)^2 - m_1^2)\theta((p_1-k)^0)\delta((p_2+k)^2 - m_2^2)\theta((p_2-k)^0)}{(k^2 - \delta_m^2)((k-q)^2 - \delta_m^2)} \ . \tag{6}$$

These integrations have been performed for electron-electron scattering in quantum electrodynamics [3], but in the

large-s limit. Here these integrals are calculated exactly, up to terms that vanish as δ_m goes to 0.

The integrations are handled by using cylindrical coordinates for k in the center-of-mass frame: i.e.,

$$k \equiv (k_0, k_\perp \cos\phi, k_\perp \sin\phi, k_z) \quad \text{and} \quad d^4k \equiv dk_0 k_\perp dk_\perp d\phi dk_z \ .$$

First the integration over ϕ is performed and then one of the δ functions is used to do the $k_\perp$ integration. The remaining δ function becomes a constraint on k_0 (in this particular case $k_0 = 0$), so only the integration over k_z remains to be done. For the simplest case ($b_{\rm cut}$) this takes the form

$$b_{\rm cut} = \frac{-i}{16\pi\rho\sqrt{\hat{s}}} \int_0^{4p^2} \frac{d\xi}{(\xi + \delta_m^2)\sqrt{[\xi^2 + 2\xi(q^2 + \delta_m^2\cos\theta) + (\delta_m^2 - q^2)^2]}} \ , \tag{7}$$

where $\xi = 2k_z p$ and $\hat{s} = (p_1 + p_2)^2$ is the square of the total center-of-mass energy of the subprocess. The integration over ξ is done analytically neglecting the terms that vanish in the zero-gluon mass limit. Equation (6) is related to the imaginary parts of the integrals via

$$2i\mathrm{Im}(b; b_\kappa; b_{\kappa\rho}) = (b; b_\kappa; b_{\kappa\rho})_{\rm cut} \ . \tag{8}$$

The resulting imaginary parts of the integrals are

$$\mathrm{Im}b = \left(\frac{\pi^3}{p\sqrt{\hat{s}}}\right) \frac{1}{q^2} \ln\left(\frac{-q^2}{\delta_m^2}\right) \ ,$$

$$\mathrm{Im}b_z = \left(\frac{\pi^3}{p\sqrt{\hat{s}}}\right) \frac{-1}{4p} \ln\left(\frac{4p^2}{\delta_m^2}\right) \ ,$$

$$\mathrm{Im}b_x = \left(\frac{\pi^3}{p\sqrt{\hat{s}}}\right) \frac{-p\sin\theta}{2} \left[\frac{1}{q^2} \ln\left(\frac{-q^2}{\delta_m^2}\right) - \frac{1}{q^2 + 4p^2} \ln\left(\frac{4p^2}{-q^2}\right)\right] \ ,$$

$$\mathrm{Im}b_{xz} = \mathrm{Im}b_{zx} = \left(\frac{\pi^3}{p\sqrt{\hat{s}}}\right) \left[\frac{1}{4}\sin\theta \ln\left(\frac{4p^2}{\delta_m^2}\right) - \frac{1}{2}\sin\theta\right] \ , \tag{9}$$

$$\mathrm{Im}b_{xx} = \left(\frac{\pi^3}{p\sqrt{\hat{s}}}\right) \left[\frac{p^2}{q^2 + 4p^2} \ln\left(\frac{4p^2}{-q^2}\right) + \frac{p^2\sin^2\theta}{2q^2} \ln\left(\frac{4p^2}{\delta_m^2}\right) + \frac{2p^2 + q^2}{4p^2}\right] \ ,$$

$$\mathrm{Im}b_{zz} = \left(\frac{\pi^3}{p\sqrt{\hat{s}}}\right) \left[\frac{q^2}{8p^2} \ln\left(\frac{4p^2}{\delta_m^2}\right) - \frac{q^2 + 2p^2}{4p^2}\right] \ ,$$

$$\mathrm{Im}b_{yy} = \left(\frac{\pi^3}{p\sqrt{\hat{s}}}\right) \left[\frac{p^2}{q^2 + 4p^2} \ln\left(\frac{4p^2}{-q^2}\right)\right] \ .$$

Integrals with other combinations of indices all vanish because of the symmetry properties of the integrand.

Note that the masses never enter explicitly in any of these results. Masses are imbedded in the kinematic definitions of $\hat{s}$, p, and q^2. Note also that there are only logarithmic terms in the scalar and vector expressions, but there are some nonlogarithmic terms in the tensor expressions. These latter will be significant in contributing nonlogarithmic terms to the polarization.

The next step requires the integrated terms be folded in with the Dirac matrices and spinors in Eq. (3). This is performed in the helicity basis by using MACSYMA, and the results, the imaginary parts of the second-order six independent helicity amplitudes (ϕ'_α) can be written as

$$\phi'_\alpha = \frac{-g^4}{16\pi p\sqrt{\hat{s}}q^2} (\lambda^a\lambda^b)_{ij} (\lambda^a\lambda^b)_{kl} \left\{\left[4(p^2 + E_1E_2) \ln\left(\frac{4p^2\sin(\theta/2)}{\delta_m^2}\right)\right] f_\alpha + g_\alpha\right\} \ . \tag{10}$$

Here f_α's are defined earlier for the lowest-order diagram and g_α's are

$$g_1 = 16\left[\left(p^2\hat{s} + m_1^2m_2^2\cos^2\frac{\theta}{2}\right) \ln\sin\frac{\theta}{2} + p^2(p^2 - E_1E_2)\sin^2\frac{\theta}{2}\right] \ ,$$

$$g_2 = -16m_1m_2\sin^2\frac{\theta}{2}\left((E_1E_2 - p^2)\ln\sin\frac{\theta}{2} + p^2\right) \ ,$$

$$g_3 = \frac{16}{\cos^2(\theta/2)}\left[\left(p^2\hat{s} - p^2(m_1^2 + m_2^2)\sin^2\frac{\theta}{2} + m_1^2m_2^2\cos^4\frac{\theta}{2}\right)\ln\sin\frac{\theta}{2} + p^2(p^2 + E_1E_2)\sin^2\frac{\theta}{2}\cos^2\frac{\theta}{2}\right] \ , \tag{11}$$

$$g_4 = 16m_1m_2\sin^2\frac{\theta}{2}\left((E_1E_2+p^2)\ln\sin\frac{\theta}{2}-p^2\right),$$
$$g_5 = -16m_1\frac{\sin(\theta/2)}{\cos(\theta/2)}\left(p^2\sqrt{\hat{s}}+E_1m_2^2\cos^2\frac{\theta}{2}\right)\ln\sin\frac{\theta}{2},$$
$$g_6 = -16m_2\frac{\sin(\theta/2)}{\cos(\theta/2)}\left(p^2\sqrt{\hat{s}}+E_2m_1^2\cos^2\frac{\theta}{2}\right)\ln\sin\frac{\theta}{2}.$$

Each amplitude has the expected dependence on quark masses and angular variables. Note that the infrared divergent term which appears only in Eq. (10) is proportional to the lowest-order amplitudes as it should be for cancellation.

Having obtained the lowest-order helicity amplitudes and the imaginary parts of the second-order helicity flip amplitudes, the next step is to calculate the leading contribution to the transverse polarization. The transverse polarization ($\mathcal{P}$) of a particle in a scattering process can be defined in terms of cross sections measured with different spin configurations of that particle: namely,

$$\mathcal{P} = \frac{[\sigma(\uparrow)-\sigma(\downarrow)]}{[\sigma(\uparrow)+\sigma(\downarrow)]}, \tag{12}$$

where the arrows denote spatial spin (up, down) configurations of the particle with respect to the scattering plane. Here spin up (down) direction is chosen to be parallel (antiparallel) to the vector $\hat{n} = \bar{p}_A \times \bar{p}_B/|\bar{p}_A \times \bar{p}_B|$.

When expressed in terms of helicity amplitudes, Eq. (12) takes the following form for the polarization of particle C of the process considered:

$$\mathcal{P} = \frac{2\,\mathrm{Im}[\Phi_5(\Phi_1+\Phi_3)^* + \Phi_6(\Phi_2-\Phi_4)^*]}{\Phi_1^2+\Phi_2^2+\Phi_3^2+\Phi_4^2+2\Phi_5^2+2\Phi_6^2}. \tag{13}$$

Finally, the substitution of helicity amplitudes into the above equation leads to the following relatively simple expression for the polarization of the scattered quark [4]:

$$P = \frac{\alpha_s\langle -1/3\rangle m_1q^2\sin(\theta/2)\{(E_2+2E_1)m_2^2\ln[\sin(\theta/2)]+E_2p^2\cos^2(\theta/2)\}}{2p\sqrt{s}\cos(\theta/2)\{2p^4\cos^4(\theta/2)+[(m_2^2+m_1^2+2E_1E_2)p^2-2p^4]\cos^2(\theta/2)+2p^4+m_1^2m_2^2\}}, \tag{14}$$

where the factor $\langle -1/3\rangle$ is the SU(3) factor for color triplets scattering on color triplets and α_s is the strong-coupling constant, which depends on the logarithm of the momentum transfer in the usual treatment of QCD. Note that the polarization is independent of infrared divergences as expected. Note also that this exact expression contains a logarithmic term in the numerator, $\ln[\sin(\theta/2)]$, and an additional contribution, $\sim[\cos(\theta/2)]$, that would not be present in a "leading log" expansion. The general form of the color factor for $s-u$ scattering can be written as

$$\left((d_{abc}+if_{abc})\frac{\mathrm{Tr}(T^aT^bT^c)}{2\mathrm{Tr}(T^{a'}T^{a'})}\right) = \frac{C_3-3C_2/2}{2C_2}, \tag{15}$$

where $C_2 = 4/3$ and $C_3 = 10/9$ for a color triplet source and $C_2 = 3$ and $C_3 = 0$ for a color octet source.

For U(1) or QED the color factor and the coupling constant have to be replaced by $\{1\}$ and α. Otherwise the formula is the same for electron (e^-)-muon (μ^-) scattering and is the same but with opposite sign for e^--μ^+ scattering. Note that the overall sign of the expression depends on whether it is a particle-particle interaction or particle-antiparticle interaction in the case of QED (in addition, the color factor is also different in the case of QCD). The sign change is a consequence in ordering fermion-antifermion fields. In the limit that the mass (m_2) of μ^+ becomes very large, compared to m_1 and p, this reduces to the polarization of electrons scattered off a spin-$\frac{1}{2}$ nucleus ($Z = 1$), the Mott asymmetry [5]:

$$P = 2\alpha\frac{m_1p\sin^3(\theta/2)\ln[\sin(\theta/2)]}{E_1^2\cos(\theta/2)[1-(p^2/E_1^2)\sin^2(\theta/2)]}. \tag{16}$$

That neglects any form factors, so is relevant for low q^2. Hence, Eq. (14), with the indicated group and coupling factors altered so that $\{\}\alpha_s \to -1\alpha Z$, provides the recoil correction to the Mott asymmetry formula for electron-nucleus scattering. Whether or not this explains slight discrepancies between the Mott formula and data [6] for scattering from $_{79}$Au remains to be checked.

Having calculated the asymmetry for $s-u$ scattering and following the above arguments, it is easy to show that the transverse polarization of the s quark from $s-\bar{u}$ scattering can be obtained from Eq. (14) by changing the overall sign and replacing the color factor by $\{7/6\}$. Therefore the final result gets the same sign for both processes and is equivalent to a scattering of an s quark on an effective color potential, which is attractive, in the limit m_2 is very large.

The other three subprocesses can be calculated by following a similar procedure. However, there is a number

of fourth-order Feynman diagrams that contribute to the imaginary part of the amplitudes of each of these subprocesses. Particularly, quark-gluon elastic scattering and gluon fusion processes involve not only a large number of Feynman diagrams but also a large number of additional integrations (b_{xxx}, b_{xxz}, etc.) due to the triple-gluon coupling vertex which makes the calculation more difficult. Feynman diagrams that contribute to the imaginary part of amplitudes and the resultant expressions for the polarization of the other processes—quark-gluon scattering, gluon fusion, and quark annihilation—are given in the following sections.

QUARK+GLUON SCATTERING

The lowest-order and the fourth-order Feynman diagrams that contribute to the imaginary amplitudes of this subprocess are shown in Figs. 2(a) and 2(b), respectively. Adding the contributions from all Feynman diagrams the following lengthy expression is obtained for the polarization of the scattered quark of mass m [4]:

$$P = \frac{\alpha_s m(E+p\cos\theta)\sin^3(\theta/2)}{6\sqrt{\hat{s}}\cos(\theta/2)D}\left\{18m^2p\sin^2\frac{\theta}{2}\left[9(E+p\cos\theta)\ln\left(\sin^2\frac{\theta}{2}\right)+2\left(E+p\cos^2\frac{\theta}{2}\right)\ln\frac{m^2}{(E+p\cos\theta)^2}\right]\right.$$
$$\left.+F\left(2p\sin^2\frac{\theta}{2}+9\sqrt{s}\right)\sqrt{s}N_1+N_2\sqrt{s}\ln\frac{E-p}{E+p}+N_3\cos\frac{\theta}{2}\right\}, \tag{17}$$

where

$$F=-\frac{1}{2\sin(\theta/2)\sqrt{E^2-p^2\cos^2(\theta/2)}}\ln\left\{\frac{E^2-p^2\cos\theta-2p\sin(\theta/2)\sqrt{E^2-p^2\cos^2(\theta/2)}}{E^2-p^2\cos\theta+2p\sin(\theta/2)\sqrt{E^2-p^2\cos^2(\theta/2)}}\right\},$$

$$N_1=2\cos^4\frac{\theta}{2}(p-E)p^2+\cos^2\frac{\theta}{2}(4Ep^2-E^2p+3E^3)-E^2(p+5E),$$

$$N_2=16\cos^6\frac{\theta}{2}(p-E)p^2+7\cos^4\frac{\theta}{2}(E^2-p^2)p+3\cos^2\frac{\theta}{2}(15p^2-14Ep+3E^2)E-(47p^2+28Ep+45E^2)E,$$

$$N_3=-2p\cos\frac{\theta}{2}\left(16p\sin^2\frac{\theta}{2}-9\sqrt{s}\right)\left(\sin^2\frac{\theta}{2}(9p+E)p-11p^2-12Ep+7E^2\right),$$

$$D=[4p^2\cos^2\theta+p(p+9E)\cos\theta+4p^2+9E(E+p)][\cos\theta(p^2+2Ep+4E^2)p$$
$$+p^3\cos^3\theta+\cos^2\theta(E^3-p^3+E^2p+2Ep^2)+p^3+2Ep^2+E^2p+E^3],$$

where E, p, and θ are the energy of the quark, the momentum, and the scattering angle, respectively. All quantities are defined in the center-of-mass frame of the subprocess. The color factors are not separately shown in the expression as in the previous case because the addition of the contributions from different diagrams with different color factors is done. The delicate cancellation of infrared divergences in the imaginary parts of loop diagrams, that must be obtained in the polarization formula, is a good test of the correctness of such a lengthy calculation. The above expression, the polarization of the scattered quark off a gluon, is distinctly different from the analogous QED expression, the polarization of the scattered electron off a photon—Compton scattering. This is mainly due to the existence of the triple-gluon coupling vertex in QCD. In the lowest order the g-g-g vertex produces a t-channel exchange and in the fourth order several new diagrams contribute as shown in Fig. 2.

By replacing the non-Abelian color factors appropriately, the corresponding scattered electron polarization in Compton scattering is obtained [4]:

$$P=\frac{\alpha m(E+p\cos\theta)\sin(\theta/2)}{p\cos(\theta/2)D'}\left(FN_1'+N_2'\ln\frac{E-p}{E+p}-\frac{2p}{\sqrt{s}}N_3'\cos^2\frac{\theta}{2}\right),$$

$$D'=(1+\cos^2\theta)[p^3\cos\theta+2Ep^2+E^2p+E^3]+p^3\sin^2\theta+2Ep(p+2E)\cos\theta,$$

$$N_1'=2p^2(p-E)\cos^4\frac{\theta}{2}+E(4p^2-Ep+3E^2)\cos^2\frac{\theta}{2}-E^2(p+5E), \tag{18}$$

$$N_2'=(p-E)\left(p\cos^2\frac{\theta}{2}-E\right)\cos^2\frac{\theta}{2}-E(p+5E),$$

$$N_3'=Ep\cos^2\frac{\theta}{2}+2(p^2+Ep+E^2).$$

However, the magnitude of the polarization is quite small. For example, the largest polarization of the scattered electron (mass $\sim$ 0.5 MeV) off a photon, which occurs when $\theta \sim 0.85$ rad and $p \sim 1.1$ MeV, is about 0.06%. For μ (mass $\sim$ 105.7 MeV) and τ (mass $\sim$ 1784 MeV) the magnitude of the polarization at the peak remains about the same as it should be due to Eq. (18) which could be written as a function of m/p. The small magnitude of the polarization is mainly due to the small value

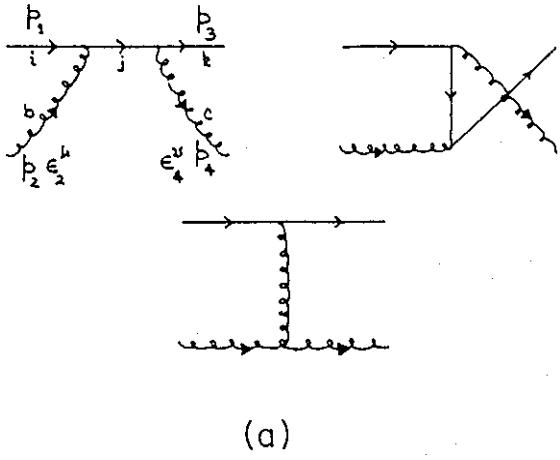

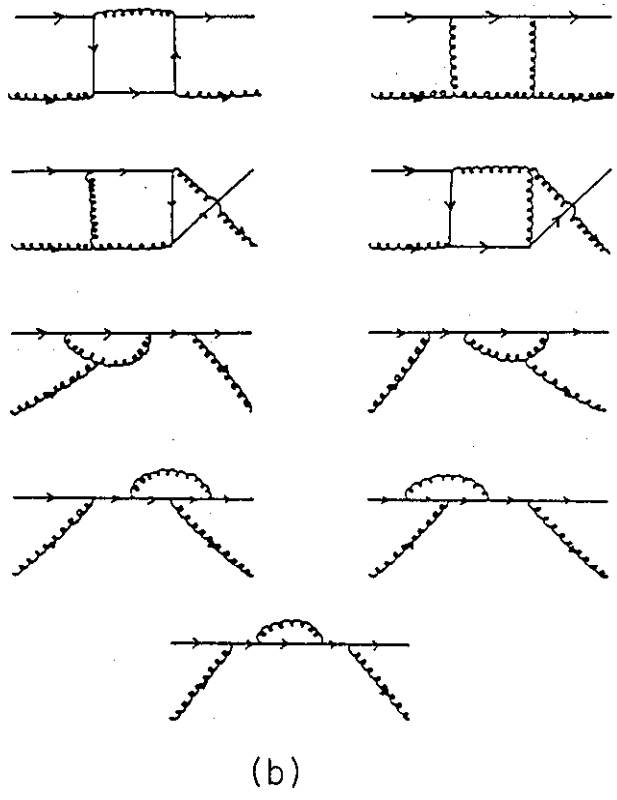

FIG. 2. Lowest-order (a) and fourth-order (b) Feynman diagrams for the $q+g \to q+g$ scattering process. In the fourth order only the diagrams which contribute to the polarization are shown.

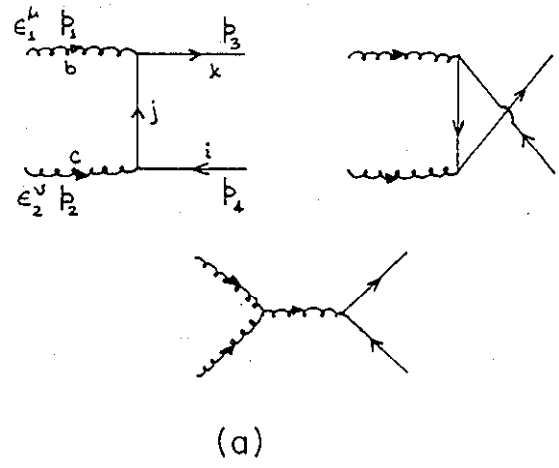

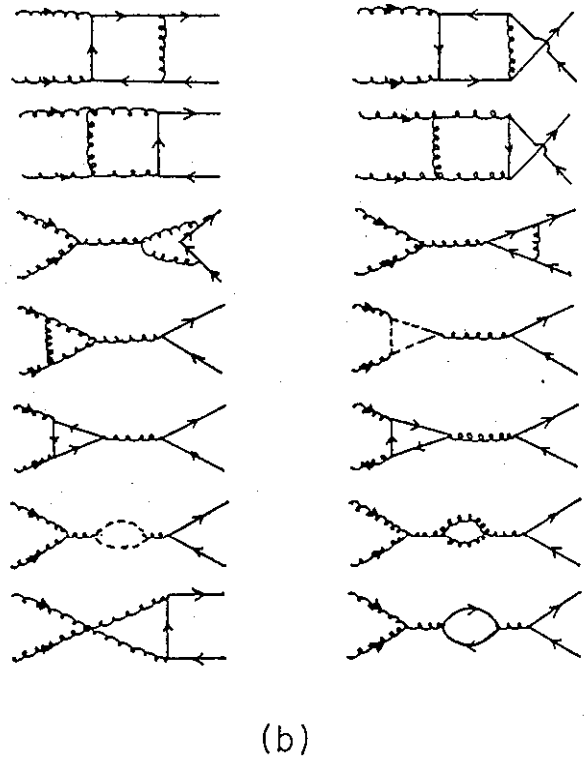

FIG. 3. Lowest-order (a) and fourth-order (b) Feynman diagrams for the gluon fusion, $g + g \to q + \bar{q}$, process. In the fourth order only the diagrams which contribute to the polarization are shown.

of the coupling constant (α) in QED. This small, order α effect would be very difficult to measure.

GLUON FUSION

The Feynman diagrams that contribute to the polarization through gluon fusion are shown in Figs. 3(a) (lowest order) and 3(b) (fourth order). Note that the existence of the triple-gluon coupling vertex produces an s-channel exchange in the lowest order. In one-loop level several new diagrams contribute to the complex amplitude which include radiative correction to the gluon propagator—"vacuum polarization." Particularly, the radiative corrections to the gluon propagator contribute to the polarization as a result of the interference with lowest order t-channel and u-channel amplitudes. This did not happen in s-g scattering since the vacuum polarization corrections to the gluon propagator are pure real in the cross channel kinematic region. Only the radiative corrections to the quark propagator contributed to the polarization of the s-quark from s-u scattering.

The resulting quark polarization for $g + g \to q + \bar{q}$ is given by [7]

$$\mathcal{P} = \alpha_s \frac{m(p^2 - k^2\cos^2\theta)}{24k\,\sin\theta D}\left((N_1+N_2)Y_+ + (N_1-N_2)Y_- + N_3\ln\frac{p-k}{p+k} + N_4 + 18k^3\sin^2\theta\cos\theta(\Sigma_1+\Sigma_2)\right), \quad (19)$$

where

$$D = (9k^2\cos^2\theta + 7p^2)(k^4\cos^4\theta - 2k^2m^2\sin^2\theta - p^4)\,,$$

$$N_1 = 9k^2\cos^3\theta(p^2+2k^2) + 6kp\cos\theta(27p^2+11kp-27k^2) + 27k^4\cos\theta\,,$$

$$N_2 = kp\cos^2\theta(11p^2+76k^2) - 162p^2m^2 + 33k^3p\,,$$

$$N_3 = p\cos\theta[243m^2p\cos^4\theta - \cos^2\theta(324m^2p-54k^3) + 22kp^2 - 243m^2p + 164k^3]\,,$$

$$N_4 = \frac{-1}{4}k\sin^2\theta\cos\theta[72\cos^2\theta(27p^3-18k^2p+k^3) + 27(96k^2p-24p^3) - 8(22kp^2+45k^3)]\,,$$

$$\Sigma_1 = \frac{2}{p^2}\sum_i \sqrt{p^2-m_i^2}(2p^2+m_i^2)\theta(\sqrt{\hat{s}}2m_i)\,,$$

$$\Sigma_2 = \frac{1}{p^2}\sum_i\left[3m_i^2p\ln\left(\frac{p-\sqrt{p^2-m_i^2}}{p+\sqrt{p^2-m_i^2}}\right) - 4(p^2-m_i^2)^{(3/2)}\right]\theta(\sqrt{\hat{s}}-2m_i)\,,$$

$$Y_\pm = \ln\left(\frac{(p\pm k\cos\theta)^2}{m^2}\right)\,.$$

This QCD polarization formula has an interesting structure, mainly due to the contribution from diagrams with internal fermion loops. m_i is the mass of the internal fermion and the summation runs over all possible intermediate quark masses. For strange quark production, as an example, m_i takes up, down, and strange quark masses at energies below the threshold for charm production. In other words an extra contribution is added to the polarization at each threshold when the center of mass energy is increased.

In the case of pair annihilation, the QED analogue of gluon fusion, the corresponding expression for the polarization of the produced lepton can be obtained by setting the QCD structure constant (f_{abc}) to zero and by replacing the other color factors by 1. The resulting expression, which is distinctly different from that of QCD, takes the form

$$\mathcal{P} = \alpha\frac{m(p^2-k^2\cos^2\theta)}{4p\,\sin\theta D'}\left[N_+Y_+ + N_-Y_- + 2\cos\theta\left((p^2+5k^2)\ln\frac{p-k}{p+k} + 2kp\cos\theta\right)\right]\,, \quad (20)$$

where

$$D' = k^4 \cos^4\theta + 2k^2p^2\cos^2\theta - 2k^4\cos^2\theta - p^4 - 2k^2p^2 + 2k^4 ,$$

$$N_\pm = \pm[(p^2 + 2k^2)\cos^2\theta + 3k^2 \pm 6kp\cos\theta] .$$

The center-of-mass variables and $Y_\pm$ are the same as above.

QUARK PAIR ANNIHILATION

Here, only the case with different flavors in the initial and in the final states is considered. Similar to gluon fusion, vacuum polarization diagrams appear in the s-channel exchange and add to the imaginary amplitude. But, they do not contribute to the polarization in this case, since they are just overall factors to the lowest-order amplitude. The lowest-order and the fourth-order Feynman diagrams that contribute to the polarization are shown in Figs. 4(a) and 4(b), respectively.

Polarization of the s quark from $u\bar{u} \to s\bar{s}$ is

$$\mathcal{P} = -\frac{\alpha_s m_2}{24p^2k^3\sin\theta D}\left[N_1 + E^4k^2m_1^2(56X_- + 16X_+) + N_2\ln\left(\frac{E+k}{E-k}\right) + N_3\ln\left(\frac{E+p}{E-p}\right)\right] , \tag{21}$$

where

$$D = 4E^4 + 2E^2(m_1^2 + m_2^2 - E^2)\sin^2\theta + 2m_1^2m_2^2\cos^2\theta ,$$

$$N_1 = -p^3k\sin^2\theta[(4k^3 + 72Em_2^2 + 36E^3)p\cos\theta + 40E^3k] ,$$

$$N_2 = E^2p[p^2m_2^2\sin^2\theta(54p\cos\theta + 20k) + k^2m_1^2(36p\cos\theta - 40k)] ,$$

$$N_3 = 4E^2pk^2m_1^2(18k\cos\theta - 5p) ,$$

$$X_\pm = \frac{p(3kp\cos\theta \pm p^2 \pm 2k^2)}{2E\sqrt{(E^2 \pm kp\cos\theta)^2 - m_1^2m_2^2}}\ln\left\{\frac{(E^2 \pm kp\cos\theta) - \sqrt{(E^2 \pm kp\cos\theta)^2 - m_1^2m_2^2}}{(E^2 \pm kp\cos\theta) + \sqrt{(E^2 \pm kp\cos\theta)^2 - m_1^2m_2^2}}\right\} ,$$

and $p(k)$ and $m_1(m_2)$ are the center-of-mass momenta and the mass of the particles in the initial (final) state, respectively, and E is the energy of the quark (or antiquark) which is the same for both initial and final states.

For the QED analogue of quark annihilation, $e^- + e^+ \to \mu^- + \mu^+$, the polarization of the produced μ^- is obtained by neglecting the diagram with the triple-gluon vertex and changing the color factors appropriately [4]:

$$\mathcal{P} = -\frac{\alpha m_2}{p^2k^2\sin\theta D}\left[N_1' + 2E^4km_1^2(X_- - X_+) + N_2'\ln\left(\frac{E+k}{E-k}\right) - 2E^2p^2m_1^2\ln\left(\frac{E+p}{E-p}\right)\right] , \tag{22}$$

where

$$N_1' = p^3k\sin^2\theta[k^2p\cos\theta - 4E^3] ,$$

$$N_2' = 2E^2p[m_2^2(E^2 - p^2\cos^2\theta) - m_1^2(E^2 + k^2)] ,$$

and the other symbols are the same as defined in Eq. (21).

The experimental verification of this formula is extremely difficult because of the small magnitude of the polarization. For example, the highest polarization of the produced μ from $e^- + e^+$ annihilation is of the order of 0.5%, which is approximately the same for heavier fermion (τ) production except the peak appears at a higher momentum.

The suppression due to the small QED coupling constant does not occur in the polarization of the produced massive quark from $e^- + e^+ \to q\bar{q}$. In this case the leading contribution to the polarization can be calculated relatively easily, since it involves only one Feynman diagram in the one-loop level. The polarization arises from the gluon radiative correction to the photon-quark vertex as shown in Fig. 4(c). Hence, the resultant polarization is proportional to the strong-coupling constant α_s. Contributions from all the other diagrams are suppressed by a factor of $\alpha_{\rm QED}$. The resultant polarization for the produced quark, in the coordinate system considered, has the simple form

$$\mathcal{P} = -\alpha_s\{4/3\}\frac{m_2k\sin\theta\cos\theta}{[2k^2(1 + \cos^2\theta) + 4m_2^2]} , \tag{23}$$

where m_2 and k are the mass and the center-of-mass momentum of the quark, respectively. $\{4/3\}$ is the resultant SU [3] color factor from quark vertices. This has been derived previously [8] in the large-Q^2 limit.

It is clear from Eq. (23) that the polarization of the quark can be written as a function of θ and m_2/k. The polarization peaks when $\theta = \pi/4$ (or $3\pi/4$) and $m_2/k \simeq 0.87$. Therefore the peak occurs above the threshold but well below the scaling region. An interesting way to relate the quark polarization to an observable quantity, assuming that the particles in the jet could remember the direction of the polarization and preferentially have a component of their momentum in that direction, has been suggested [8]. Also, a more careful description of fragmentation of transversely polarized quarks, as given in [2], for example, can be used to obtain observable quantities. However, Eq. (23) predicts less than 5% asymmetry at the best.

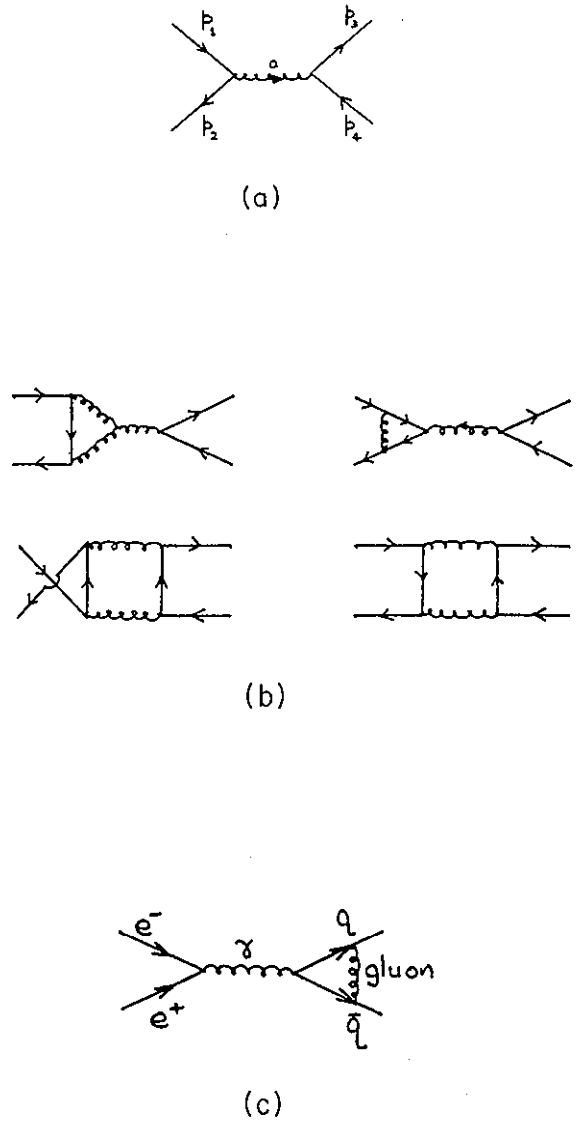

FIG. 4. Lowest-order (a) and fourth-order (b) Feynman diagrams for the annihilation, $q + \bar{q} \rightarrow q' + \bar{q}'$, process. In the fourth order only the diagrams which contribute to the polarization are shown. (c) The most significant Feynman diagram for the polarization of massive quark through $e^+ + e^-$ annihilation.

KINEMATICAL DEPENDENCE OF THE POLARIZATION

The magnitude of the polarization depends on several variables. The scattering angle, θ, and the momentum or the energy in the center-of-mass frame can be varied independently. Hence, we need to study the variation of the polarization with these two variables. Furthermore, to estimate the polarization from the full QCD formula, one needs quark masses and the strong-coupling constant α_s. What quark mass—current, constituent, or perhaps a larger effective mass incorporating confinement effects at lower energies where the perturbative QCD is partially valid—should be inserted? Spontaneous symmetry breaking of chiral invariance, incorporating instanton effects in the vacuum, have been evoked to give quark propagators mass corrections [9]. The effective mass that arises for one quark flavor is momentum dependent, as anticipated, and gives expected "constituent" values at low momentum.

It is an interesting point to mention that the polarization expressions can be written as functions of α_s, θ, and m_i/p, eliminating the other parameters by using the kinematical relations. This shows that the properties of polarization can be discussed for any given quark mass; for a higher mass the same properties will appear at a higher momentum. Hence, for simplicity, the constituent quark masses, 0.3, 0.5, 1.5, and 4.5 GeV/c^2 for up (or down), strange, charm, and bottom quarks, respectively, are used when necessary. Also, a constant value, $\alpha_s = 0.4$, is used for the strong-coupling constant which is an overall factor in the polarization.

The kinematical dependence of the polarization of the outgoing strange quark in the center-of-mass frame is shown in Figs. 5(a)–5(d) for the four subprocesses. The polarization as a function of θ is shown for different values of center-of-mass momentum (the region of the momentum is chosen to study the polarization at the peak). For large momentum relative to quark masses the polarization still becomes negligible as expected. However, for relatively low momenta there is a considerable structure. The first two subprocesses, $s+u$ and $s+g$ scattering, produce smaller polarization compared with the other two. It should be pointed out that the full expression for the polarization is significantly distinct from that of the leading logarithmic approximation, as an example the sign change in the polarization from $s + u$ is a consequence of the additional contribution from the nonlogarithmic term in the expression.

Another interesting thing to study is the quark mass dependence of the polarization. For $s + u$ scattering this is done by expressing the polarization as a function of θ, $x = m_s/p$, and $y = m_u/p$. Figure 6(a) shows the x and y dependence of the polarization at the peak which occurs at $\theta \simeq 130°$. Although the parameters x and y

are expressed in terms of strange and up quark masses, the result could be read for the scattering of any two quarks of different flavor. The sign of the polarization is determined by the parameter y. For small values of y the polarization is positive and it peaks when $y = 0$ and $x \simeq 1.5$. For large y, the sign changes and the largest negative polarization ($\sim -5.5\%$) occurs when $y \to \infty$ at $x \simeq 0.4$, i.e., the polarization gets its largest negative value if the s quark is scattering off a static color source. For a color octet static source the polarization is still negative and it is $\sim -12\%$ at the peak.

For the $s+g$ scattering, most of the features, peaks, and the sign changes, are very similar to the previous case. The major difference is that the largest negative polarization occurs at moderate momenta ($p \sim 1600$ MeV/c) and the positive peak exists at smaller values of $p \sim 200$ MeV/c. Therefore the kinematic regions in which the two different subprocesses change sign and peak do not coincide. However, those regions could overlap when smeared by relevant quark and gluon structure functions. The quark mass dependence of the polarization is easy to study here, since this process involves only one quark. The polarization as a function of the center-of-mass scattering angle (θ) and m/p is shown in Fig. 6(b). Although there are several bumps and dips, the overall magnitude is smaller than in the previous case. Again, the magnitude is largest when $\theta \simeq 130°$, i.e., in the backward scattering and the sign changes with m/p. The sign at the peak changes from negative to positive when m/p increases from ~ 0.35 to ~ 2.0. For larger m/p it becomes negative again and peaks at $\theta \simeq 85°$.

The quark polarization from gluon fusion is more interesting than the two subprocesses discussed above; the magnitude is comparatively larger and it remains significant for larger values of center-of-mass momenta. The estimation of the s-quark polarization involves not only the strange quark mass but also the other quark masses which could be excited depending on the available energy. The polarization vanishes [Fig. 5(c)] at $\theta = \pi/2$ and the sign changes leaving the magnitude the same under $\theta \to \pi - \theta$ as one expects from constraints on helicity amplitudes under identical particle interchange. The quark mass dependence of the polarization at the peak, i.e., at $\theta \simeq 60°$, is shown in Fig. 6(c). The variation with the final-state quark mass (m) and with the gluon center-of-mass momentum (p) is given. The constituent quark

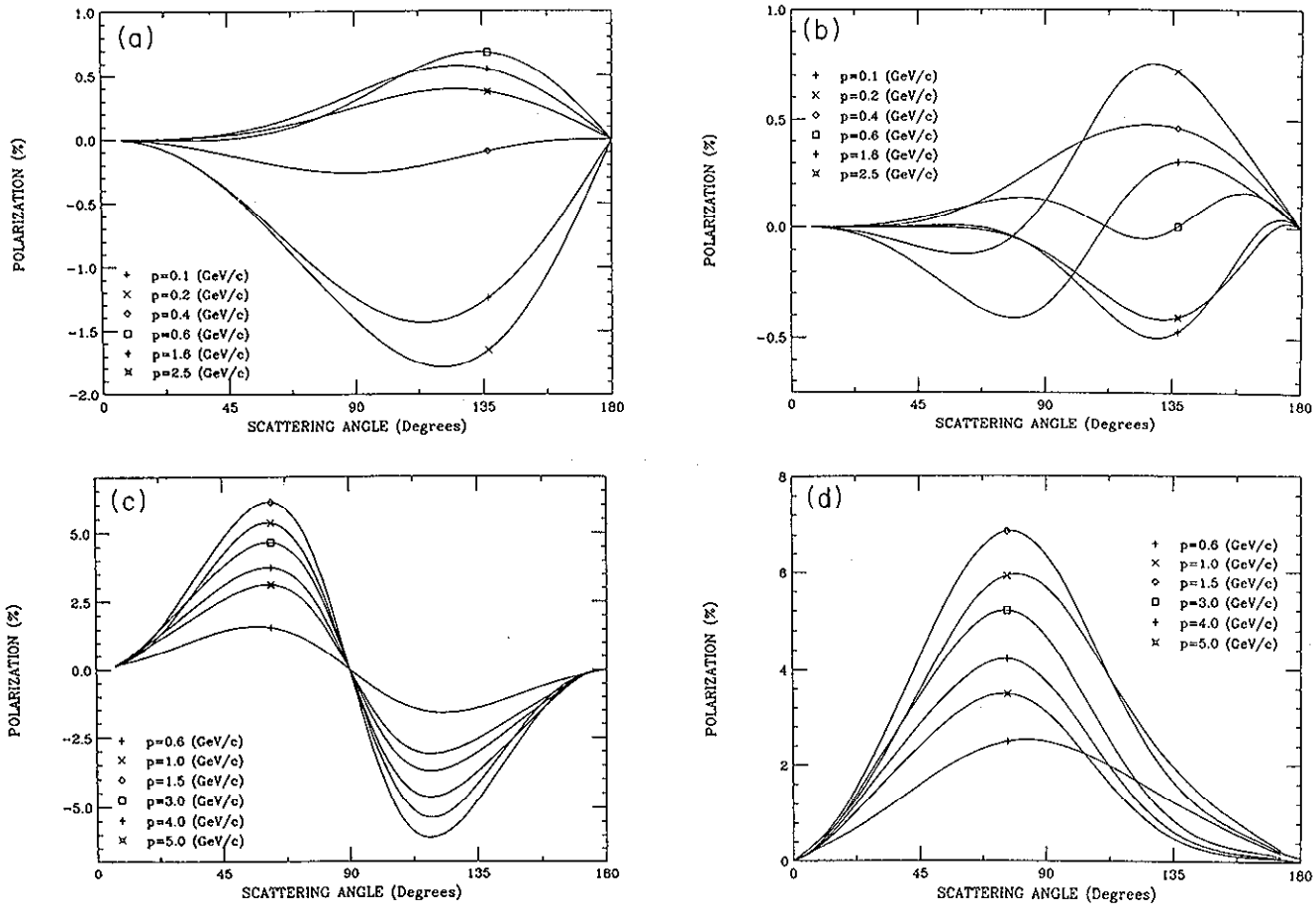

FIG. 5. Polarization of outgoing s quark in the subprocess center-of-mass frame as a function of the scattering angle with $\alpha_s = 0.4$, $m_u = m_d = 0.3$ GeV/c^2, $m_s = 0.5$ GeV/c^2, $m_c = 1.5$ GeV/c^2, $m_b = 4.5$ GeV/c^2. (a) $q+q' \to q+q'$, (b) $q+g \to q+g$, (c) $g+g \to q+\bar{q}$, and (d) $q+\bar{q} \to q'+\bar{q}'$.

masses are used for all internal fermion loops and the numerical result is almost the same if they are replaced by current quark masses. Note that the magnitude of the highest polarization remains the same while the peak gets broader when m increases. The peak occurs when $m/p \simeq 0.3$. More interesting is the momentum structure of the polarization. For small momenta, polarization increases rapidly with p until the peak value is reached and then decreases slowly, a slower rate than one would expect from a leading logarithmic approximation in m/E. The new terms that are added to the polarization at each threshold of pair production, when p increases, are partially responsible for that effect.

It is an interesting point to mention, even though an individual Feynman diagram is not a gauge-invariant entity, that the dominant contribution to the polarization comes from one particular diagram, namely from the radiative corrections to the gluon propagator—"vacuum polarization." This appears in the s-channel exchange and contributes to the imaginary parts of amplitudes in gluon fusion, in contrast to the gluon propagator corrections in the t-channel exchange for $s+u$ and $s+g$ scattering subprocesses with no contribution to the imaginary amplitudes. That imaginary amplitude contributes to the polarization as a result of the interference with the lowest order t- and u-channel amplitudes. The existence of the diagram with an s-channel intermediate gluon, for the subprocesses considered, is a result of the

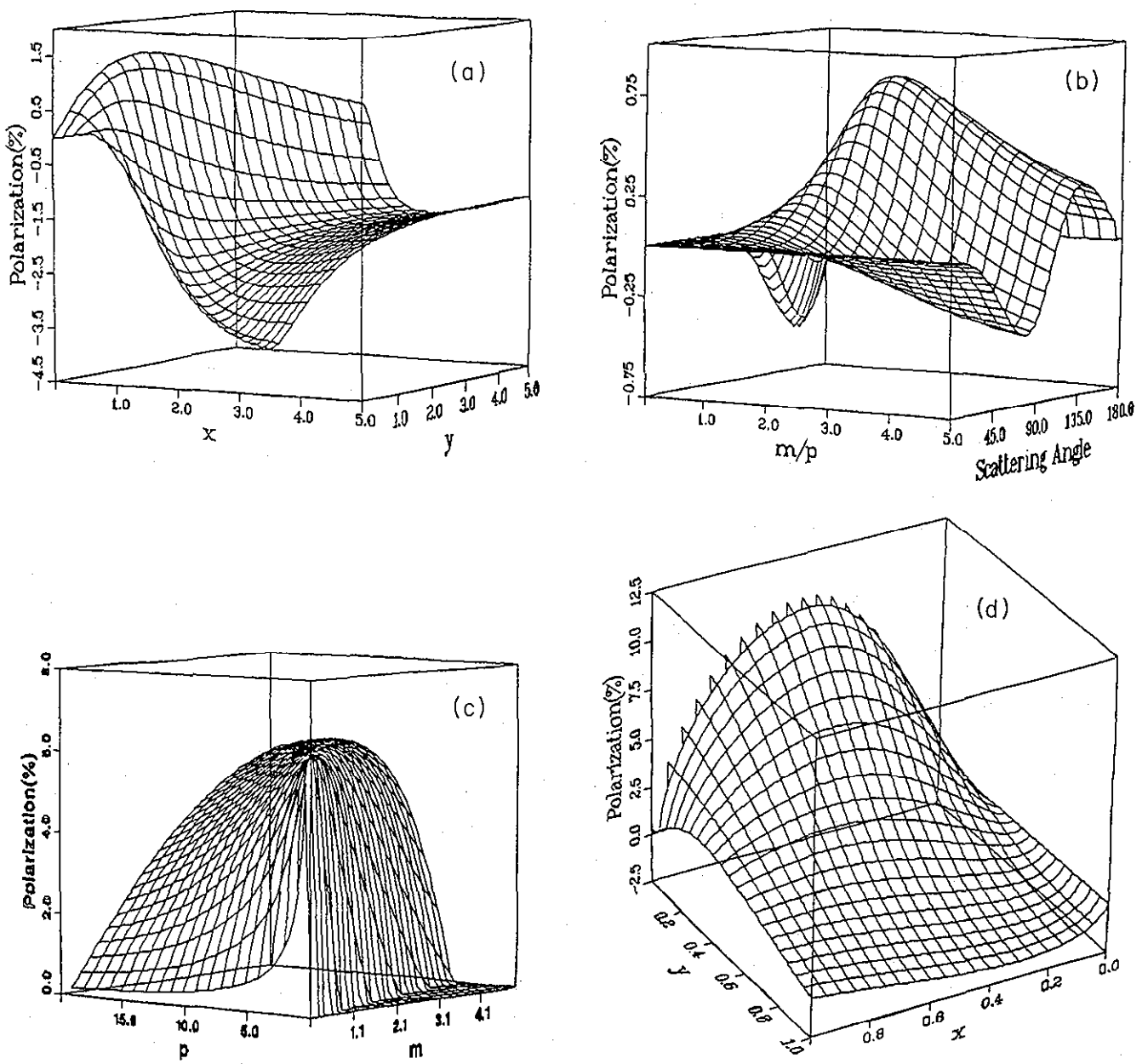

FIG. 6. Mass dependence of the polarization of the outgoing s quark. All parameters are the same as in Fig. 5. (a) $q+q' \to q+q'$, (b) $q+g \to q+g$, (c) $g+g \to q+\bar{q}$, and (d) $q+\bar{q} \to q'+\bar{q}'$.

non-Abelian character of the theory which makes the polarization large and distinct from the analogous QED expression.

The polarization of the s quark produced from the quark annihilation [Fig. 5(d)] has interesting characteristics which are similar to those from gluon fusion. Namely, the magnitude is large and the highest polarization occurs at reasonably larger center-of-mass momenta. Interestingly, the region in the parametric space, p and θ, at which the polarization peaks is the same for these two subprocesses. This will certainly help to minimize the dilution of the polarization in the addition of the two contributions within the convolution integrals. For the values of parameters chosen the polarization is always positive and it peaks at $p \simeq 1.5$ and $\theta \simeq 80°$. The magnitude is slightly larger than all the other processes. More interesting is the quark mass dependence of the polarization which can be parametrized as a function of $x = m_s/p$ and $y = m_u/p$, where m_u and m_s are the initial-state (u-quark) and the final-state (s-quark) quark masses. x and y dependences of the polarization at the peak, i.e., at $\theta \simeq 80°$, is shown in Fig. 6(d). Note that the kinematical constraint for pair production, $\hat{s} > 4m_s^2$, leads to $1 + y^2 > x^2$. While the magnitude is quite small and the x dependence is insignificant for large y, there is a reasonable structure for small y which is the region that produces heavier quarks from lighter quark annihilation. The largest polarization (10.5%) occurs at $x \simeq 0.5$ and smallest possible y, i.e., $y = 0$ or for massless quarks in the initial state.

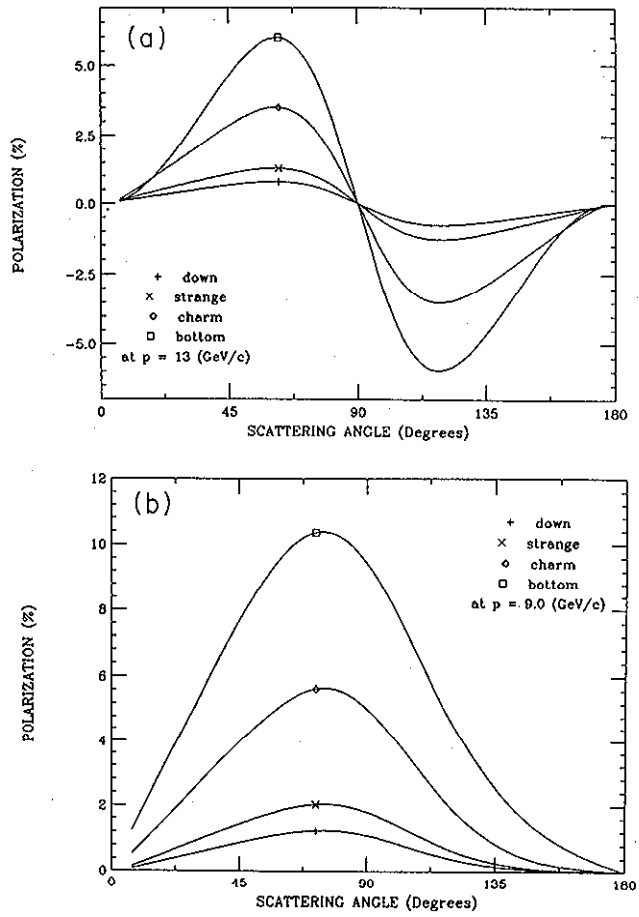

FIG. 7. Polarization of up, strange, charm, and bottom quarks at the subprocess CM momentum of (a) 13 GeV/c for gluon fusion and (b) 9 GeV/c for annihilation. Other parameters are identical to Fig. 5.

HEAVY-QUARK POLARIZATION

It is interesting to pursue the possibility of heavy quarks, charm, or bottom quarks, becoming polarized in the production processes. It is well known [10] that the heavy-quark production cross section is dominated by the gluon fusion subprocess, especially at large transverse momenta and small Feynman x, while the annihilation processes give the next significant contribution. This general rule is true as long as the beam or the target does not carry any valence heavy quarks, because, then the heavy-quark contribution to the structure functions is negligible. Therefore, the first two subprocesses, the flavor excitation processes, are not considered for heavy-quark production.

The polarization of down, strange, charm, and bottom quarks from gluon fusion are compared in Fig. 7(a). Here, the center-of-mass momentum of gluons is chosen ($p = 13$ GeV/c) to obtain the largest polarization for the bottom quark. As can be seen by comparing with Fig. 5(c) the overall magnitude of the polarization has not increased for heavy quarks, but at a given momentum the heaviest quark acquires the largest polarization. This is always true if the center-of-mass energy is well above the threshold for pair creation. For heavy-quark production from $u + \bar{u}$ annihilation, the result is very similar and is shown in Fig. 7(b). Here, the center-of-mass momentum of the u quark is chosen to be $p = 0.9$ GeV/c to see the peak of bottom quark polarization. Again, the heaviest quark gets the largest polarization at a given momentum as in the previous case. In addition, the magnitude at the peak gets larger for heavier quarks. For example, the peak polarization for bottom quarks is about $\sim 10\%$ while that for strange quarks is about 7%. This is due to the fact that for heavier quarks the peak polarization occurs at a higher momentum which lowers the value of the quantity y in Fig. 6(d) moving the kinematical region towards the peak of the polarization. However, once we go to the higher momentum the effects of the decreasing coupling constant have to be taken into account, and that is an overall factor.

TOP QUARK POLARIZATION

The study of the polarization properties of the top quark, when its mass is near or above 120 GeV, is more interesting for several reasons and worth giving special consideration. As has been already discussed in detail [11,12] the physics of the top quark has distinctly different features from other quarks, especially in its polarization phenomena. The main interesting feature for the

spin physics of the top quark is the rapidity of its decay process. First, the depolarization mechanism effective for other quarks does not play a role for the heavy top quark and, second, it decays as a free quark with no hadronization or recombination effects due to its rapid decay [11]. So, any polarization information carried by the produced top quark should be directly transferred into its decay products with neither dilution nor enhancement. Furthermore, the dominant decay process of the top quark, the electroweak two-body decay $t \to bW^+$, will be an ideal analyzer of its own polarization.

The transverse polarization of the top quark from gluon fusion and quark annihilation subprocesses are shown in Figs. 8(a) and 8(b) for a top quark of mass 140 GeV/c^2. The constituent quark masses given earlier are used for the other quarks. Note that the top quark polarization from gluon fusion depends on all the other quark masses due to the contribution from the vacuum polarization diagram. The approximate value of the running coupling constant, $\alpha_s = 0.15$, is used in the estimation of the magnitude. Although the magnitude is small, $\sim 2\%$ from gluon fusion and $\sim 4\%$ from annihilation at the peak with the above value of the α_s, it is not zero even in the kinematic region where the perturbative QCD is expected to be valid with no doubt. This is an even more interesting result to verify experimentally, if it is possible, since the predicted polarization arises from the one-loop level but not as a correction to the leading-order predictions. This is a direct test of the fourth-order prediction from perturbative QCD.

By using the polarization formula for gluon fusion, published previously [7], an interesting method to test the top quark polarization at the CERN Large Hadron Collider (LHC) has been suggested in [12]. At the LHC energies, the top quark production is dominated by the gluon fusion subprocess and the next significant contribution comes from the annihilation subprocess [12]. Having obtained the polarization from annihilation processes, one can include both subprocesses' polarization in the convolution with the quark and gluon distribution functions to obtain the resultant polarization for the appropriate hadron collider, which is neglected in [12].

Since the top quark has been observed at Fermilab, it may be possible to collect a few hundred top events (if the expected luminosity is reached) before the LHC to study the physics of the top quark. At the Fermilab Tevatron energies the annihilation subprocess plays the dominant role in the production of the heavy top quark. Therefore, the polarization of the top quark through the annihilation process is more significant here. As a result, the resultant polarization of the top quark at Tevatron energies is slightly larger than that of LHC. The significance of the top quark polarization at the Fermilab Tevatron has been discussed already [13]. However, in the discussion of the single-spin asymmetry perpendicular to the scattering plane, the contribution from $q\bar{q}$ subprocesses, which is given here, should be included in order to obtain the upper bound for observable effects due to the standard theory. Then, any sizable asymmetries observed can be incorporated into new physics.

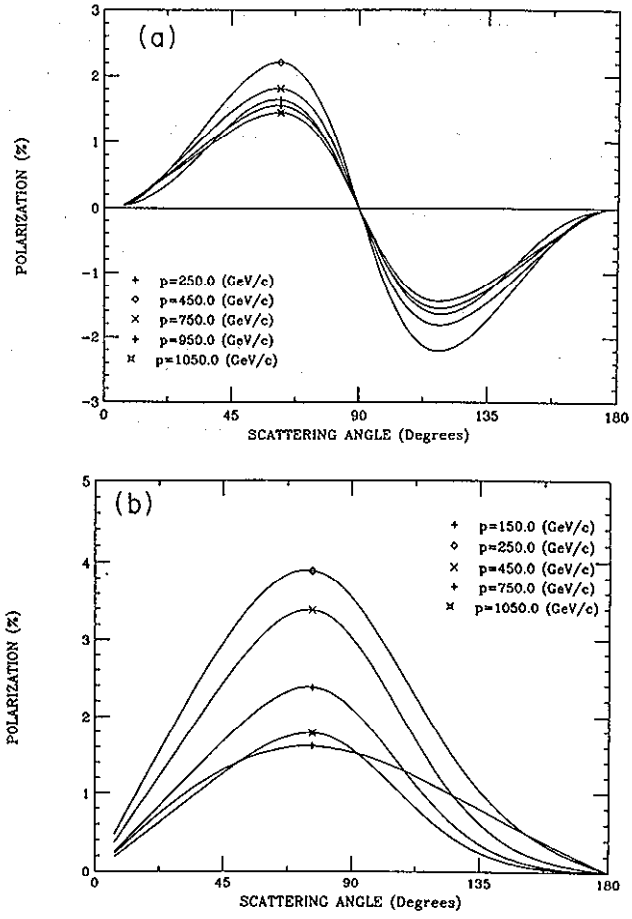

FIG. 8. Polarization of the top quark of mass 140 GeV/c^2, (a) from gluon fusion and (b) from annihilation. Other parameters are identical to Fig. 5 except $\alpha_s = 0.15$.

It is an interesting point to mention that the large transverse polarization in inclusive hyperon production processes, which involve the strange quark production, observed previously (see references in [7]) will not occur here since the top quark is produced at very high energy and it decays very rapidly—the polarization of the top quark is preserved as discussed above. Therefore, any observation of top quark polarization larger than the predictions given here will be an indication of some new or nonstandard model interactions, which could happen at high energies where the top quark is produced. This makes the measurement of the top quark polarization very important and interesting experimentally as well as theoretically.

Note added in proof. An error in N_4 of Eq. (19) was brought to our attention by A. Brandenberg [14] to whom we are grateful.

ACKNOWLEDGMENT

This work was supported in part by a grant from the U.S. Department of Energy.

[1] R. H. Dalitz, G. R. Goldstein, and R. Marshall, Phys. Lett. B **215**, 783 (1988); G. R. Goldstein, in *High Energy Spin Physics: Eighth International Symposium*, Proceedings, Minneapolis, Minnesota, 1988, edited by K. J. Heller, AIP Conf. Proc. No. 187 (AIP, New York, 1989).
[2] J. Collins, Nucl. Phys. **B396**, 161 (1993), and references contained therein.
[3] R. N. Cahn and Y. S. Tsai, Phys. Rev. D **2**, 870 (1970).
[4] W. G. D. Dharmaratna, G. R. Goldstein, and G. A. Ringland, Z. Phys. C **41**, 673 (1989). (Note: The sign error has been corrected here.)
[5] W. A. Mckinley and H. Feshbach, Phys. Rev. **74**, 1759 (1948); R. H. Dalitz, Proc. R. Soc. London **A206**, 509 (1951); A. I. Akhiezer and V. B. Berestetskii, *Quantum Electrodynamics*, 3rd ed. (Nauka, Moscow, 1969).
[6] P. E. Spivak *et al.*, Sov. Phys. JETP **14**, 759 (1962).
[7] W. G. D. Dharmaratna and G. R. Goldstein, Phys. Rev. D **41**, 1731 (1990).
[8] G. L. Kane *et al.*, Phys. Rev. Lett. **41**, 1689 (1978).
[9] D. I. Dyakonov and V. Yu. Petrov, Nucl. Phys. **B272**, 457 (1986).
[10] P. D. B. Collins and A. D. Martin, *Hadron Interactions* (Hilger, London, 1985).
[11] R. H. Dalitz and G. R. Goldstein, Phys. Rev. D **45**, 1531 (1992).
[12] G. L. Kane, G. A. Ladinsky, and C. -P. Yuan, Phys. Rev. D **45**, 124 (1992).
[13] G. A. Ladinsky, Phys. Rev. D **46**, 3789 (1992).
[14] W. Bernreuther, A. Brandenberg, and P. Uwer, Aachen Report No. PITHA 95/26, 1995 (unpublished).